Journal of King Saud University – Engineering Sciences (2018) 30, 183–187

King Saud University

Journal of King Saud University – Engineering Sciences

www.ksu.edu.sa
www.sciencedirect.com

ORIGINAL ARTICLE

Investigation of surface residual stress profile on martensitic stainless steel weldment with X-ray diffraction

I.I. Ahmed [a,*], J.A. Adebisi [b], S. Abdulkareem [c], A.H. Sherry [a]

[a] Material Performance Centre, University of Manchester, Oxford Road, Manchester M13 9PL, UK
[b] Department of Materials and Metallurgical Engineering, University of Ilorin, P.M.B. 1515, Nigeria
[c] Department of Mechanical Engineering, University of Ilorin, P.M.B. 1515, Nigeria

Received 22 September 2015; accepted 19 January 2016
Available online 25 January 2016

KEYWORDS

Residual stress;
Weld;
Stainless steel;
X-ray;
HAZ

Abstract The development of residual stresses during fabrication is inevitable and often neglected with dire consequences during the service life of the fabricated components. In this work, the surface residual stress profile following the martensitic stainless steel (MSS) pipe welding was investigated with X-ray diffraction technique. The results revealed the presence of residual stresses equilibrated across the weldment zones. Tensile residual stress observed in weld metal was balanced by compressive residual stresses in the parent material on the opposing sides of weld metal.

1. Introduction

The welding of 13% MSS is characterised by phase changes and transformation of austenite, γ to hard and brittle martensite (Griffiths et al., 2004; Spencer et al., 2009; Turnbull and Griffiths, 2003; Woollin et al., 1999). The transformation is accompanied by a significant expansion of up to 1% in volume, coupled with thermal distortion and weld shrinkage, which collectively lead to rise in the level of residual stresses in the pipe (Castro-López and De Cadenet, 1975). Although, the plate like shape of martensite structure has the capability to accommodate the transformation strains and thus provides cushion for this effect (Bhadeshia, 2004; Jones and Alberry, 1978).

Residual stresses occur as a result of misfit between different components in an assembly during manufacturing processes which include welding and fabrication (Thibault et al., 2009). The nature and magnitude of residual stresses in components is dependent on the key material properties namely: coefficient of thermal expansion, heat capacity, density and strength (Bhadeshia, 2004; Mazahery and Shabani, 2013). On a macro scale, the production of seam pipe by progressive folding of plate into circular shape and subsequently welding along the longitudinal axis often introduce residual stresses in the pipe. Whereas on micro scale, microstructures have different responses to temperature change because of the

* Corresponding author at: Department of Materials and Metallurgical Engineering, University of Ilorin, P.M.B. 1515, Ilorin, Nigeria. Tel.: +234 7018271354.
E-mail address: ismaila.ahmed@yahoo.com (I.I. Ahmed).
Peer review under responsibility of King Saud University.

Production and hosting by Elsevier

http://dx.doi.org/10.1016/j.jksues.2016.01.004

difference in their Coefficient of Thermal Expansion (CTE), for instance, the CTE of austenite, γ in steel is about $2.1E{-}06\ K^{-1}$ while that of ferrite, α is approximately $1.3E{-}06\ K^{-1}$ (Bhadeshia, 2004).

Residual stresses introduced by the manufacturing processes can be reduced to minimise their effects during service life. Seamless pipe have little or no internal stresses because of its complementary stress relief annealing during hot working processes. Other methods used include the application of pressurised water to longitudinally welded seam pipe after fabrication (Hanneman et al., 1979) and shot peening using different methods (Dieter and Bacon, 1986; Ling et al., 2008). And, in situations where welding is involved, Post Weld Heat Treatment (PWHT) may be necessary to mollify the consequences of internal residual stresses in the weldment (Dong et al., 2014).

The Gas Metal Arc Welding (GMAW) is one of the welding processes often used for joining martensitic stainless steel pipes to achieve required transportation networks over a long distance (Woollin, 2007; Asahi et al., 1999). It is a very versatile welding process due to the fact that its deposition mode could either be in droplets, spray or globular transfer mode which allows out of position welding to be carried out (DeGarmo et al., 2003; Schmid and Kalpakjian, 2006). In GMAW, the externally supplied shielding gas played dual roles. Firstly, it protects the arc, the molten metal and cooling weld metal from impurities in the air and secondly, it provides desired arc characteristics through its effect on ionisation (Messler, 2008). In addition, welding could be carried out with power source biased towards the DC-Electrode Negative, DC-EN or DC Reverse Polarity, DCRP which is the same as DC-EP mode, depending on the wire used and desired mode of molten metal transfer. The DC-EP is most commonly used because electrons are accelerated from negative work piece onto the positive electrode with sufficient energy to melt the filler wire (Messler, 2008). The aim of this work is to investigate the surface residual stresses in martensitic stainless steel pipe weldment. This was achieved by carrying out surface residual stress measurements on girth welded martensitic pipes, using the X-ray diffraction technique.

2. Experimental procedure

2.1. Materials

The materials used for the research study was low carbon martensitic stainless steels. The materials were provided as-welded by The Welding Institute (TWI), Cambridge, United Kingdom. The original martensitic stainless steel pipe without any welding heat input is referred to as the parent steel and the filler wire used for fabrication was superduplex stainless steel. The detailed chemical compositions of the parent and filler metals are shown in Table 1.

2.1.1. Girth welding of MSS pipes

Mechanised Pulsed Gas Metal Arc (PGMA) welding process was used for the fabrication of the MSS pipes at TWI, Cambridge. The PGMA welding process is notable for significantly lower welding porosity. The Gas-metal arc welding process used 1.2 mm diameter superduplex stainless steel (MW4) (Table 1) as continuous filler wire electrode and an externally supplied inert shielding gases (comprising $Ar/He/CO_2/N_2$) against oxidation and for better control of weld puddle. The consumable wire electrode produced an arc with the work piece which formed a part of the electric circuit and provided filler to the weld joint. Wire was fed to the arc by an automatic wire feeder.

A typical schematic diagram of the weldment is shown in Fig. 1. The three distinct structural zones that exist in the weldment as characterised by the welding heat are: the parent material, the HAZ and the weld metal affected by dilution during high temperature fusion. The transverse sections of girth welded low carbon, MSS pipe was sectioned out for investigation. The sample nomenclature was W2B.

2.2. X-Ray diffraction technique

The $\sin^2\psi$ method of X-ray diffraction technique is applicable for plane stress condition, and was therefore used to determine the magnitude of the residual stress to the depth of about 20 μm in the as-welded specimen. The X-ray diffraction method for lattice strain measurement relies on well established Braggs law illustrated with Eq. (1), where λ is the X-ray wavelength, d is the interatomic lattice spacing and θ is the diffraction angle (Cullity and Stock, 2001; Fitzpatrick et al., 2005).

$$\lambda = 2d\sin\theta \tag{1}$$

The technique measured elastic stress from diffraction elastic constants determined from measurable elastic strains, assuming linear elastic distortion occured in the contributing crystal lattice plane. The lattice elastic strain for the reflections (h k l) at angle ψ are calculated from shift in interatomic lattice spacing (Fig. 2) caused by manufacturing process according to Eq. (2). The lattice spacing, d is obtainable from wave length and diffraction angle, 2θ according to Eq. (2). The d_o is the stress free lattice spacing and the $d\psi$ is the measured stressed lattice spacing (Fitzpatrick et al., 2005).

$$\varepsilon_{\psi}^{(hkl)} = \frac{d_{\psi}^{(hkl)} - d_o}{d_o} \tag{2}$$

In plane stress condition (where the in-plane stress, $\sigma_z = 0$) and considering that biaxial stresses exist, then the tensile force which produces a strain along X direction will have a lateral effect consistent with Hooke's law and the ratio of transverse to longitudinal strains defines the Poisson ratio, υ according the Eq. (3)

Table 1 Chemical composition of the specimens used (parent metal and the filler wire).

Description	Element, wt%									
	C	N	Si	Mn	P	Ti	Cr	Mo	Ni	Al
Parent steels	0.009	0.005	0.20	0.43	0.014	0.120	12.20	2.51	6.40	0.03
Filler (1.2 mm ϕ)	0.027	0.232	0.40	0.41	0.016	NA	26.10	3.90	9.30	NA

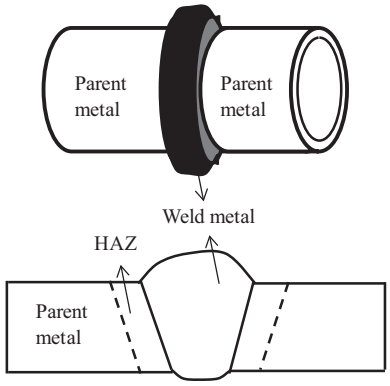

Figure 1 Typical schematic diagram of weldment showing parent metal, HAZ and weld metal.

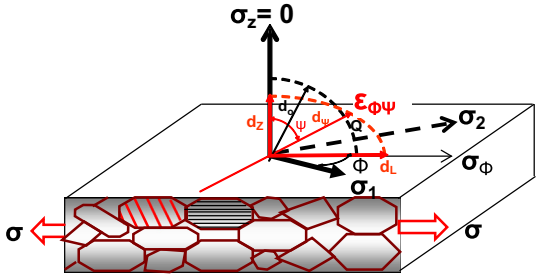

Figure 2 Schematic illustration of change in interatomic lattice spacing, d (Cullity and Stock, 2001).

$$\varepsilon_x = \varepsilon_y = -v\varepsilon_z = \frac{-v\sigma_y}{E} \tag{3}$$

At the near surface of material, where the X-ray measurement is carried out, $\sigma_z = 0$ and the corresponding strain is calculated from Eq. (4),

$$\varepsilon_z = -v(\varepsilon_x + \varepsilon_y) = \frac{-v}{E}(\sigma_x + \sigma_y) \tag{4}$$

$$\varepsilon_{\emptyset\psi} = \frac{1+v}{E}\left(\sigma_1 \cos^2 \emptyset + \sigma_2 \sin^2 \emptyset\right) \sin^2 \psi - \frac{v}{E}(\sigma_1 + \sigma_2) \tag{5}$$

$$\sigma_\emptyset = \frac{E}{(1+v)\sin^2 \psi}\left(\frac{d_\psi - d_n}{d_n}\right) \tag{6}$$

$$\sigma_\emptyset = \left(\frac{E}{1+v}\right)m \tag{7}$$

The elasticity theory for an isotropic solid shows that the strain along the angle, ψ could be obtained from Eq. (5). The Eq. (6) enables the calculation of the stress in any chosen direction from the lattice spacings determined from two measurements, made in a plane normal to the surface and containing the direction of the stress to be determined.

The portable diffractometer used for X-ray diffraction was Proto residual stress analyser. The diffractometer uses Croto computer software for data processing and analysis of results. It used Cr Kα_2 radiation, which has wavelength of 2.2897 Å as X-ray anode. The diffraction angle of the radiation was 156.1°. Body Centre Cubic lattice and crystallographic planes, {2 1 1} were used for martensitic stainless steel specimen. Transverse residual stresses at six different points across weld were considered for measurement.

3. Results and discussion

The X-ray diffraction technique was used to determine residual stresses in the weldment. The plot of intensity of radiation against Bragg angle 2θ is shown in Fig. 3. The Gaussian curve fitting was done for the determination of the peak value of Bragg angle at each measurement location. The plot of lattice spacings (see Eq. (1)) against $\sin^2\psi$ (the tilt angle) and the determination of the slope of the curve (Fig. 4) from which stress was calculated were all done with Croto software. It will be observed from Fig. 4, the lattice spacings data for the crystallographic plane (2 1 1) was considered because it is the most representative of the bulk martensitic stainless steels. Again, splitting of $\sin^2\psi$ occured on the plot as indicated by values of detector 1 and 2 and line of best fit was drawn for the determination of intercept from which stress was calculated. The splitting of lattice spacing against $\sin^2\psi$ plots could be attributed to shear stress components not been zero, thus resulting in different values of lattice spacings at positive and negative values of ψ (Fitzpatrick and Lodini, 2003; Balasingh and Singh, 2000). The uncertainties in the measurement may also arise from the effects of large grain size particularly in the weld metal.

During the XRD measurement, several measurements were made at different tilt angles, ψ, and the plot of lattice spacings (calculated from Eq. (1)) against $\sin^2\psi$ is shown in Fig. 4. The stress is then calculated from the gradient and existing diffraction elastic constant of the material. Assuming the stress is zero when lattice spacing, $d = d_n$, where d is the intercept on the y-axis when $\sin^2\psi = 0$, from the gradient, m of the plot in Fig. 4, the stress is therefore calculated from Eq. (7).

Table 2 shows the values of residual stresses calculated using $\sin^2\psi$ method. Table 2 shows the x and y coordinate positions of the sample on the goniometer for every point on the weldment measured. The values of residual stresses and the error values are also shown in the Table 2.

Points 1 and 2 which are on the LHS of the weld metal (Fig. 5) exhibit compressive residual stresses with negative values of −298 and −122 MPa respectively. The weld metal which corresponds with point 3 exhibits tensile residual stress with positive value, 369.5 MPa. On the right of the weld metal, points 4, 5 and 6 show compressive residual stresses with

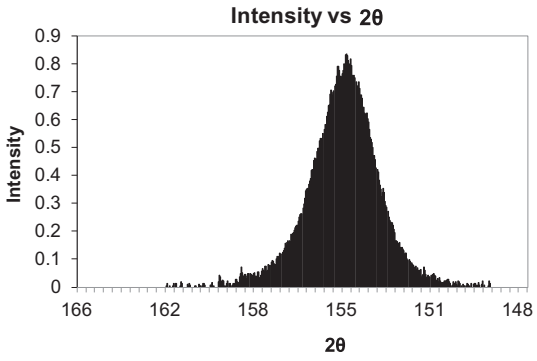

Figure 3 Plot of intensity against diffraction angle 2θ.

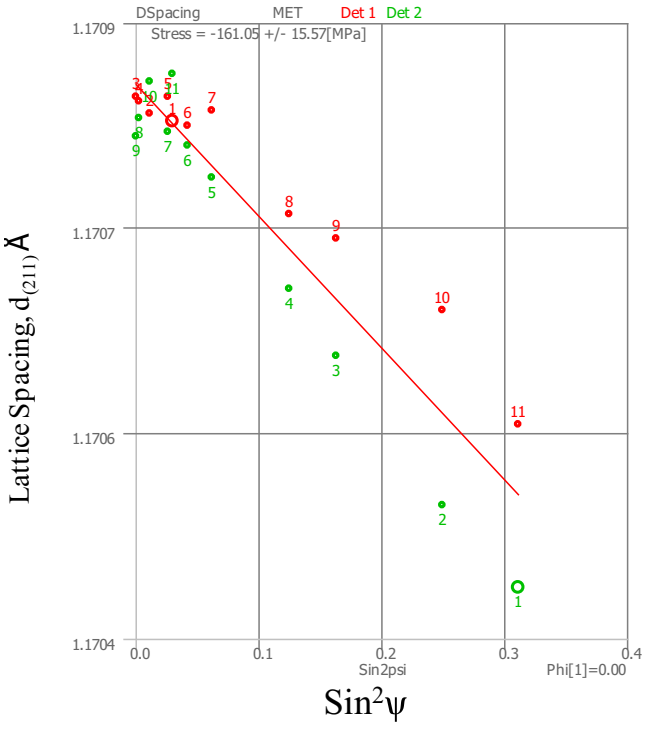

Figure 4 Linear dependence of lattice spacing of reflection (2 1 1) upon $\sin^2\psi$.

Table 2 Table of value of residual stresses carried out on as-welded specimen.

No.	Measurement positions (at $\phi = 0$)		Transverse stress (MPa)	Error
	X	*Y*		
1	−26.08	−28.85	−298.10	38.91
2	−23.93	−28.85	−122.28	17.69
3	−19.74	−28.85	369.50	112.36
4	−15.69	−28.85	−148.61	23.12
5	−13.06	−28.85	−92.03	22.90
6	−10.35	−28.85	−162.58	19.53

negative values of −148.6, −92.03 and −162.5 MPa respectively. The error values for each stress values are also shown in Table 2.

Points 1 and 2 which are on the LHS of the weld metal (Fig. 5) exhibit compressive residual stresses with negative values of −298 and −122 MPa respectively. The weld metal which corresponds with point 3 exhibits tensile residual stress with positive value, 369.5 MPa. On the right of the weld metal, points 4, 5 and 6 show compressive residual stresses with negative values of −148.6, −92.03 and −162.5 MPa respectively. The error values for point 3 is particularly higher compared to other stress values in Table 2, this is consistent with large grain size effect of the weld metal. Relatively larger grain size occurs in the weld metal due to grain growth caused by prolonged cooling after welding (Ahmed et al., in Press).

Fig. 5 shows the graph of residual stress in transverse direction against the measurement locations on the weldment placed adjacent to the graph. As shown in the graph, the

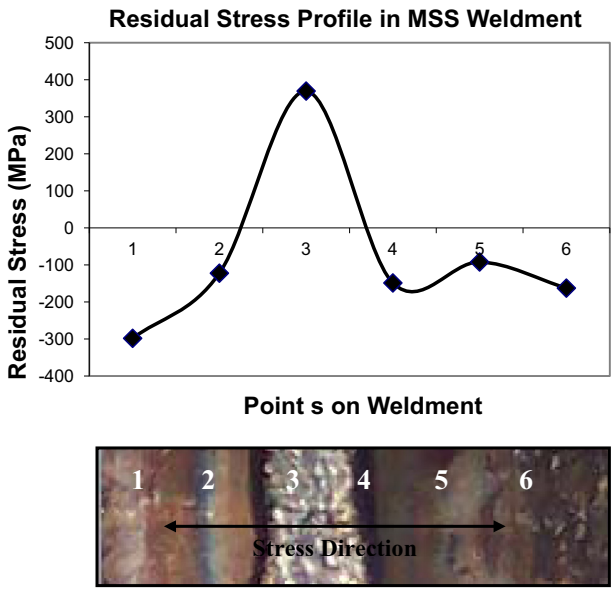

Figure 5 Residual stresses profile in martensitic stainless steel weldment.

parent material on the LHS of the weld metal showed a compressive residual stress. However, there was a gradual rise in residual stress value from parent material towards the weld metal across the HAZ region.

It is supposed that, some part of the HAZ region on both sides of the weld close to the parent material have compressive residual stress, while the remaining parts within the neighbourhood of the fusion boundaries showed gradual rise in stress values towards the weld metal. The weld metal shows tensile residual stress.

The result of transverse residual stress from Table 2 showed that compressive residual stress occurred in the parent material while some part of HAZ and the weld metal have tensile residual stress. Ideally, the value of residual stress fluctuates with an error value of ±50. Therefore, the results of the residual stress measured with X-ray diffraction and its error values were consistent with convectional residual stress profiles obtainable from weldment due to thermal stress. It must be mentioned however, that the error value for weld metal was greater than +50, the reason for this was because of the coarse nature of the weld metal. The value of residual stress is strongly dependent on the particular grain that makes the largest contribution to the diffraction peak. The amount of intensity observed by the counter is affected by the coarseness of the grain. The implication of large grain size is low density of diffracting grains required to produce smooth intensity distribution in the peak (Fitzpatrick et al., 2005).

Residual stresses occurred in the weldment because of mismatch caused by the temperature gradient during the process of welding (Balasingh and Singh, 2000). When the weld metal was in the molten state, the expansion of the liquid metal is prevented by relatively colder parent material with significantly higher yield strength and this will result in high temperature plastic deformation in the weld metal. However, during cooling after welding, the weldment and HAZ contracts as the temperature reduces, but the contraction in the weld and HAZ is restrained by the colder parent material therefore causing tension in the HAZ and the weld metal. The net effect is

tensile residual stress in the weld metal and HAZ which is balanced by compressive residual stress in the parent material.

Again, It was discovered that superduplex stainless steel wire used to fill the weld metal contained high amount of carbon and nitrogen with propensity for diffusion across the narrow fusion boundary into the neighbouring heat affected zone (with an initial relatively low concentration). The resulting carbon and nitrogen enrichment of the heat affected zone closed to the fusion boundary and the weld cap has the capability to cause increase in hardness value and the strength of the regions, and consequently the tensile residual stress observed in the regions (Alphonsa et al., 2015; Ahmed et al., in Press).

The presence of tensile residual stress in the HAZ is a source of concern in area of applications susceptible to stress corrosion cracking (SCC). Tensile residual stress may act as a crack opener particularly in the HAZ region which has a higher susceptibility to failure by SCC in MSS.

4. Conclusion

The following conclusions are made at the end of the study aimed at determining the surface residual stress profile on martensitic stainless steel weldment with X-ray diffraction.

(i) Residual stress levels measured showed compressive residual stress in the parent material and tensile residual stress in some parts of heat affected zone close to the fusion boundaries and in the weld metal, where the stress was tensile and indeed, a maximum.
(ii) The results are consistent with the conventional residual stress profile in girth weldments.
(iii) Compressive residual stress is beneficial in applications susceptible to SCC since it acts to close the crack, and in contrast, tensile residual stresses act as crack opener thus providing a sustainable crack driving force.
(iv) The high hardness and strength in the weld metal cap and fusion boundary neighbourhood, consequent upon higher C and N in the filler wire could be attributed to tensile residual stress in the region.

Acknowledgement

The authors wish to thank Judith Shackleton for her supports during the X-ray diffraction test at Manchester Materials Science Centre.

References

Ahmed, I.I., Adebisi, J.A., Taiwo, T., Abdulkareem S., Sherry, A.H., in Press. Microstructural correlation of hardness profile in martensitic stainless steel weldment. J. Metallogr. Microstruct. Anal. http://dx.doi.org/10.1007/s13632-015-0254-9.

Alphonsa, J., Raja, V.S., Mukherjee, S., 2015. Study of plasma nitriding and nitrocarburizing for higher corrosion resistance and hardness of 2205 duplex stainless steel. Corros. Sci. 100, 121–132.

Asahi, H., Nose, K., Inoue, H., Tmehiro, H., Terasawa, T., Koyuba, M., Ayukawa, N., 1999. Corrosion and mechanical properties of weldable martensitic stainless line pipes. Supermartensitic Stainless Steels 99, 27–28.

Balasingh, C., Singh, A., 2000. Residual stresses and their measurements by X-ray diffraction methods. Met. Mater. Process. 12, 269–280.

Bhadeshia, H.K.D.H., 2004. Developments in martensitic and bainitic steels: role of the shape deformation. Mater. Sci. Eng. A 378, 34–39.

Castro-López, R., De Cadenet, J.J., 1975. Welding Metallurgy of Stainless and Heat-Resisting Steels. CUP Archive.

Cullity, B.D., Stock, S.R., 2001. Elements of X-ray Diffraction. Prentice Hall, Upper Saddle River, NJ.

Degarmo, E.P., Black, J., Kohser, R.A., Klamecki, B.E., 2003. Materials and Process in Manufacturing. John Wiley and Sons, USA, 974.

Dieter, G.E., Bacon, D., 1986. Mechanical Metallurgy. McGraw-Hill, New York.

Dong, P., Song, S., Zhang, J., 2014. Analysis of residual stress relief mechanisms in post-weld heat treatment. Int. J. Press. Vessels Pip. 122, 6–14.

Fitzpatrick, M., Fry, A., Holdway, P., Kandil, F., Shackleton, J., Suominen, L., 2005. Determination of residual stresses by X-ray diffraction. In: Measurement Good Practice. National Physical Laboratory, Teddington.

Fitzpatrick, M.E., Lodini, A., 2003. Analysis of Residual Stress by Diffraction Using Neutron and Synchrotron Radiation. Tailor & Francis, London.

Griffiths, A., Nimmo, W., Roebuck, B., Hinds, G., Turnbull, A., 2004. A novel approach to characterising the mechanical properties of supermartensitic 13 Cr stainless steel welds. Mater. Sci. Eng. A 384, 83–91.

Hanneman, R.E., Rao, P., Danko, J.C., 1979. Intergranular stress corrosion cracking in 304 SS BWR pipe welds in high temperature aqueous environments. Environment-Sensitive Fracture of Engineering Materials, Chicago, Illinois, 153–177.

Jones, W., Alberry, P., 1978. Model for stress accumulation in steels during welding. In: Proc. Conf. on Residual Stresses in Welded Construction and Their Effects, 1978, pp. 15–26.

Ling, X., Ni, H.F., Ma, G., 2008. Investigation of the influence of shot peening on stress corrosion cracking of stainless steel welded joints. Mater. Sci. Forum, 672–677 (Trans Tech Publ).

Mazahery, A., Shabani, M.O., 2013. Plasticity and microstructure of A356 matrix nano composites. J. King Saud Univ. Eng. Sci. 25, 41–48.

Messler, R.W., 2008. Principles of Welding: Processes, Physics, Chemistry, and Metallurgy. Wiley.

Schmid, R., Kalpakjian, S., 2006. Manufacturing Engineering and Technology. Pearson Prentice Hall, Upper Saddle River, NJ.

Spencer, K., Conlon, K., Brechet, Y., Embury, J., 2009. The strain induced martensite transformation in austenitic stainless steels: Part 2 Effect of internal stresses on mechanical response. Mater. Sci. Technol. 25, 18–28.

Thibault, D., Bocher, P., Thomas, M., 2009. Residual stress and microstructure in welds of 13% Cr–4% Ni martensitic stainless steel. J. Mater. Process. Technol. 209, 2195–2202.

Turnbull, A., Griffiths, A., 2003. Review: corrosion and cracking of weldable 13 wt% Cr martensitic stainless steels for application in the oil and gas industry. Corros. Eng. Sci. Technol. 38, 21–50.

Woollin, P., 2007. Welding supermartensitic stainless steels for corrosive service. In: Stainless Steel World Conference, Maastricht, Holanda, pp. 6–8.

Woollin, P., Noble, D.N., Lian, B., 1999. Weldable 13% Cr martensitic steels for pipeline applications: preliminary studies. In: EPRG/PRCI 12th Biennial Joint Technical Meeting on Pipeline Research.